Meteorology and Atmospheric Physics (2022) 134:70
https://doi.org/10.1007/s00703-022-00911-8

ORIGINAL PAPER

Tropical cyclones in the northern Mozambique Channel: composite intra-seasonal forcing and 2019 event

Mark R. Jury[1,2] · Corene J. Matyas[3]

Received: 19 August 2020 / Accepted: 20 June 2022 / Published online: 12 July 2022
© The Author(s), under exclusive licence to Springer-Verlag GmbH Austria, part of Springer Nature 2022

Abstract

Tropical cyclone (TC) activity in the northern Mozambique Channel (nMC) during the satellite era is studied, culminating with the anomalous 2019 season. We identify 21 westward-moving TCs since 1979 and analyze regional to local conditions as they move over the nMC. As easterly flow is needed to steer these TC into the channel and over land, we look for scenarios under which this flow is established along with thermodynamic conditions necessary to support TCs. At seasonal scales there is a dichotomy between westward steering flow and reduced thermodynamic energy during Pacific La Niña and cool-phase Indian Ocean Dipole (–IOD). Equatorial convective systems (Madden Julian Oscillation, MJO) entering the west Indian Ocean can trigger TC formation and subtropical ridging, more effectively at the end of austral summer. Conditions in early 2019 favoured westward flow over Madagascar. The onset of warm phase + IOD was evident in the Walker circulation and downwelling ocean Rossby wave that warmed SST to 31 °C north of Madagascar. High-amplitude MJO triggered the genesis of TCs Idai (March) and Kenneth (April) and both TCs transited the Mozambique Channel causing unprecedented floods. TC Kenneth intensified rapidly, and satellite rainfall and upper level ozone indicated the presence of a southern spiral cloud band that shielded the TC from the sub-tropical jet over Madagascar. Numerical model forecasts of track and intensity are evaluated.

1 Introduction

Islands and coasts around the Mozambique Channel are vulnerable to tropical cyclone (TC) impacts. Environmental conditions in this region are favourable to TC development in austral summer (~ 9/yr) from December to April (Wang et al. 1998; Emanuel and Nolan 2004; Mavume et al. 2009; Leroux et al. 2018). Most TCs of the southwest Indian Ocean recurve poleward in the longitudes 45–60°E (Mudenda and Mumba 2004; Reason 2007; Jury 2013). Although a significant threat to maritime activities (Jury et al. 1993; Jury et al. 1998; Chang Seng and Jury 2010a,b) only 5% of TCs forming northeast of Madagascar make landfall further west in Mozambique (Vitart et al. 2003; Reason and Kiebel 2004; Malherbe et al. 2012). Yet TC Kenneth did so in 2019 and motivates our work to discover how westward steering flow develops in the region.

At the inter-annual timescale, the leading coupled climate mode of the tropical Indian Ocean is the east–west dipole (Saji et al. 1999; Webster et al. 1999; Xie et al. 2001; Yeshanew and Jury 2007; Luo et al. 2010; Izumo et al. 2010). The Indian Ocean Dipole (IOD) reflects a zonal seesaw of the tropical thermocline coupled with regional winds (Jury and Huang 2004; Cretat et al. 2018; Jury 2018a). Unlike the slower equatorial Pacific, IOD amplitude is greatest south of the equator in Oct–Jan season (Schott et al. 2009). As the thermocline deepens near Madagascar, sea temperatures increase > 1 °C and TCs are 2–3 times more frequent (Chikoore et al. 2015; Burns et al. 2016). The IOD links with Pacific El Niño Southern Oscillation (ENSO) to alter steering flow in the Mozambique Channel, inducing one-quarter of TCs to move westward during La Niña and negative IOD phase (Matyas 2015). For example, the 2000 TC season saw several westward tracks (Dyson and van Heerden 2001) associated with a deep sub-tropical ridge

Responsible Editor: Clemens Simmer.

✉ Mark R. Jury
mark.jury@upr.edu

[1] Geography Department, University of Zululand, KwaDlangezwa 3886, South Africa

[2] Physics Department, University of Puerto Rico, Mayaguez 00681, USA

[3] Geography Department, University of Florida, Gainesville, FL 32611, USA

and Pacific La Niña (Vitart et al. 2003; Mavume et al. 2009; Malherbe et al. 2013; Fitchett and Grab 2014). In contrast, Pacific El Niño induces westerly shear and fewer TCs with poleward tracks (Vermeulen 1995; Jury et al. 1998; Ho et al. 2006; Chang-Seng and Jury 2010a; Matyas and Silva 2011). Our research considers how IOD phase affects TC movement across the northern Mozambique Channel.

At the intra-seasonal timescale the Madden–Julian Oscillation (MJO; Madden and Julian 1994) can alter TCs around the Mascarene Islands (Bessafi and Wheeler 2006); more so when the inter-tropical trough shifts toward the equator. Ho et al. (2006) found that convective circulations accompanying MJO entering the Indian Ocean (phase 2–3) trigger TCs near Madagascar, while MJO approaching the Maritime Continent (phase 4) induce westward steering flow (Kiladis et al. 2014). Although one-third of MJO do not reach sufficient amplitude to affect West Indian Ocean climate, most MJO interact with IOD and Pacific El Niño (Cretat et al. 2018). We follow up, to learn how MJO alter tropical cyclogenesis and steering flow.

Anticipating a season of above normal TCs with westward tracks toward northern Mozambique would help identify coastal zones that should make pre-storm preparations. Although coupled models can predict IOD phase and its convection, the steering flow is more difficult (McIntosh and Hendon 2018; Lin 2019). Thus, an observational study of conditions surrounding westward-moving TCs in the northern Mozambique Channel (nMC) is warranted. As the majority of TCs entering the nMC recurve, we consider model forecasts for westward tracks such as TC Kenneth.

The 2019 season was characterized by frequent cyclogenesis over the West Indian Ocean (10–20°S, 40–60°E) and three TCs making landfall over Mozambique. The World Health Organization (WMO 2019) estimated that floods displaced 420,000 + people contributing to ~ 1000 deaths. Reliefweb (2019) reports that in the Comoros islands, TC Kenneth displaced 19,000 + people. These impacts motivate our research and extend earlier studies on active TC seasons (Poolman and Terblanche 1984; Malherbe et al. 2011; Chikoore et al. 2015).

The aim of this paper was to analyze the characteristics of TCs in the nMC from December to April, extending work of Matyas (2015) that examined TCs further south. We study the conditions associated with TCs moving westward over the nMC during the past 40 years. After inter-annual and intra-seasonal variations are explored, a case study is presented and short-range forecasts of structure, track and intensity are qualitatively analyzed. Scientific questions include the following: (i) what seasonal and intra-seasonal features induce westward TCs in the nMC? (ii) Are the features globally or locally forced and (iii) what made the 2019 TC season so anomalous?

2 Data and methods

TC tracks and intensity are drawn from the National Ocean and Atmospheric Administration (NOAA CSC) Coastwatch IBTrACS database in the satellite era 1979–2019 with a focus on westward moving cases in Dec–Apr covering the area: 7–17°S, 40–50°E, hereafter denoted as the 'nMC'. We use a two-step screening to isolate TCs in this area as follows: (i) TC tracks longer than 500 km heading 210–300° and (ii) TCs with highest (ranked) wind speed and rainfall. The two-step screening yielded 21 cases over 40 years. Cattiaux et al. (2020) describe a more complex scheme to track TCs in ERA5 reanalysis over the 5 month season (their Figs. 7,10).

In situ data are scarce in the nMC, so we rely on remote sensing inputs from the National Aeronautics and Space Administration (NASA) and the coupled global data assimilation system to describe the structure and evolution of TCs. The data (listed in Table 1) include the following: satellite SST, net outgoing longwave radiation (OLR), vegetation fraction, soil moisture, near-surface sea temperature, currents, waves, winds, vertical motion, air temperature, humidity, rainfall, and upper level ozone. Reanalysis fields derive from the Climate Forecast System v2 (CFS2; Saha et al. 2010), the European Community Reanalysis v5 (ERA5; Hersbach et al. 2020), the Famine Early Warning System land data assimilation system (FLDAS; McNally et al. 2017), the Global Ocean Data Assimilation System (GODAS; Behringer 2007), the Hybrid Coordinate Ocean Model (HYCOM3; Hurlburt et al. 2009), the NASA Modern-era Reanalysis for Research Applications (MERRA2; Rienecker et al. 2011; Molod et al. 2015), the Simple Ocean Data Assimilation (SODA3; Carton et al. 2018) and the National Centers for Environmental Prediction (NCEP2; Kanamitsu et al. 2002). Where products overlap, the higher resolution is used to better represent the TC–environment interactions (Cattiaux et al. 2020).

Reanalysis with a fine resolution $\leq 0.25°$ such as hourly CFS2 and ERA5 have sufficient detail for extraction of the following TC indices within the nMC area: (i) maximum wind speed, (ii) maximum rainfall and (iii) minimum central pressure. Reanalysis having a coarse resolution $\geq 0.5°$ is used for regional thermodynamic and kinematic fields and ocean conditions. Moving from 1979 to 2019 seasonal statistics to the Kenneth case study, NDBC buoy measurements at 8°S, 55°E (McPhaden et al. 2009) are obtained in the Jan–Apr 2019 period. Wind gust measurements from Mayotte airport (FMCZ) 12.8°S, 45.2°E are compared with reanalysis data during TC passage. TC track and intensity forecasts for Kenneth are drawn from Navy COAMPS-TC (Doyle et al. 2014) for multiple models including COTC and HWRF and compared with satellite rainfall from cMorph and GPM products

Table 1 Datasets used in the analysis

Dataset	Acronym	Parameters	Resolution
Climate Forecast System v2 reanalysis	CFS2	Wind gust, maximum rainfall, minimum central pressure	0.25° hourly
CPC Morphed satellite precipitation	cMorph	Estimated rainfall	0.25° 3-hourly
European Community Reanalysis v5	ERA5	Winds, rainfall, sea level pressure	0.25° hourly
FEWS land data assimilation system	FLDAS	Reanalysis soil moisture	0.1° daily
Global Ocean Data Assimilation System	GODAS	Reanalysis sea temperature, currents, vertical motion, sea level	0.5° pentad
Global Precipitation Measurement (satellite + gauge)	GPM	Estimated rainfall	0.1° 3-hourly
Hybrid Coordinate Ocean Model	HYCOM3	Ocean reanalysis near-surface currents, sea temperature	0.1° daily
Mayotte airport observations	FMCZ	Wind gusts at 12.8°S, 45.2°E, 7 m	Station hourly
Modern-era Reanalysis for Research Applications v2	MERRA2	Specific humidity, winds, upper level ozone	0.5° 6-hourly
National Aeronautics & Space Admin. satellite products	NASA	Net outgoing longwave radiation (OLR), SST, vegetation fraction	0.1°– 0.5° daily
National Centers for Environmental Prediction v2 reanalysis	NCEP2	Vertical section of atmospheric circulation	1.8°daily
National Data Buoy Center	NDBC	Buoy observations from the Rama site at 8°S, 55°E	Station hourly
National Oceanic & Atmospheric Admin. Coastwatch	NOAA	Reanalysis of TC tracks and intensity	0.1° 3-hourly
Simple Ocean Data Assimilation v3	SODA3	Reanalysis wind stress, currents	0.5° monthly
US Navy TC analysis tool	COAMPS-TC	Track/intensity forecasts (multi-model)	0.1° 3-hourly
Wave Analysis Model v3 reanalysis	WAM3	Ocean significant wave height, direction, period	0.5° 3-hourly

(Joyce et al. 2004; Huffman et al. 2007; Hou et al. 2014). Ocean swell characteristics are analyzed from the Wave Analysis Model (WAM3; Tolman et al. 2002). Most of these data are delivered through websites listed in the acknowledgements. Our work compares with Mawren et al. (2020) and offers further insights on local – regional interactions.

Temporal indices are formulated for inter-annual statistical analysis 1979–2019 using Pacific ENSO Nino3.4 SST, southern oscillation index (SOI) and IOD represented by sub-surface sea temperatures (as derived in Appendix Fig. 9a). We employ standard indices for the MJO analysis 1979–2019 which use daily satellite net OLR values for a 15° × 15° area over the equator centered on 20°E (Africa) and 70°E (Indian O.), filtered to retain 36–48 day periods (as in Kiladis et al. 2014). Inter-annual lag correlations are computed + /–6 months with respect to Dec–Apr nMC 500 hPa U wind; these have 40 degrees of freedom (1/yr) and require $r^2 > 0.10$ or $r > |.31|$ to achieve 95% confidence. Intra-seasonal lag correlations are computed + /–24 days in seasonal bins for Africa with respect to Indian MJO OLR; these daily MJO-filtered time series have > 100 degrees of freedom and require $r^2 > 0.05$ or $r > |.22|$ to achieve 95% confidence. For analysis of composite anomalies 1979–2019, seasonal and daily data are ranked to extract cases based on the following three criteria: (i) Dec-Apr westward steering flow, (ii) deep convection in the nMC and (iii) westward TC events.

Outcomes evolve from long to short time-scales and regional to local space-scales: (i) Dec–Apr seasonal climate 1979–2019 covering the period with most frequent TCs, (ii) seasonal correlations with global indices, (iii) daily composite anomalies of 21 west-moving TCs, (iv) MJO influence (cf. Kiladis et al. 2014) based on equatorial OLR indices over Africa (20°E) and the Indian Ocean (70°E) with 36–48 day periods, (v) anomalous nature of Jan–Apr 2019 season, (vi) hourly analysis of Kenneth passing the Comoros and (vii) forecasts of TC Kenneth 23–25 Apr 2019. We focus on air-sea interactions before / during TC passage in the nMC; impacts after landfall in Mozambique are further studied in Mawren et al. (2020).

3 Results

3.1 Seasonality

In the period 1979–2019, 57 TCs passed through our study area. Although storm motion spans a range of directions due to weak steering flow (Matyas 2015), half moves towards 210–300° with an average translation speed of 4.1 m/s.

The marine climatology of the nMC TC season (De–Apr) is illustrated in Fig. 1a–d. This region is located between equatorial northerly monsoon and subtropical trade wind climates (Fig. 1a). Easterlies prevail east of Madagascar, but in the Mozambique Channel the airflow is meridional and converging into the inter-tropical trough. The mountains that span Madagascar deflect the summer trade winds causing

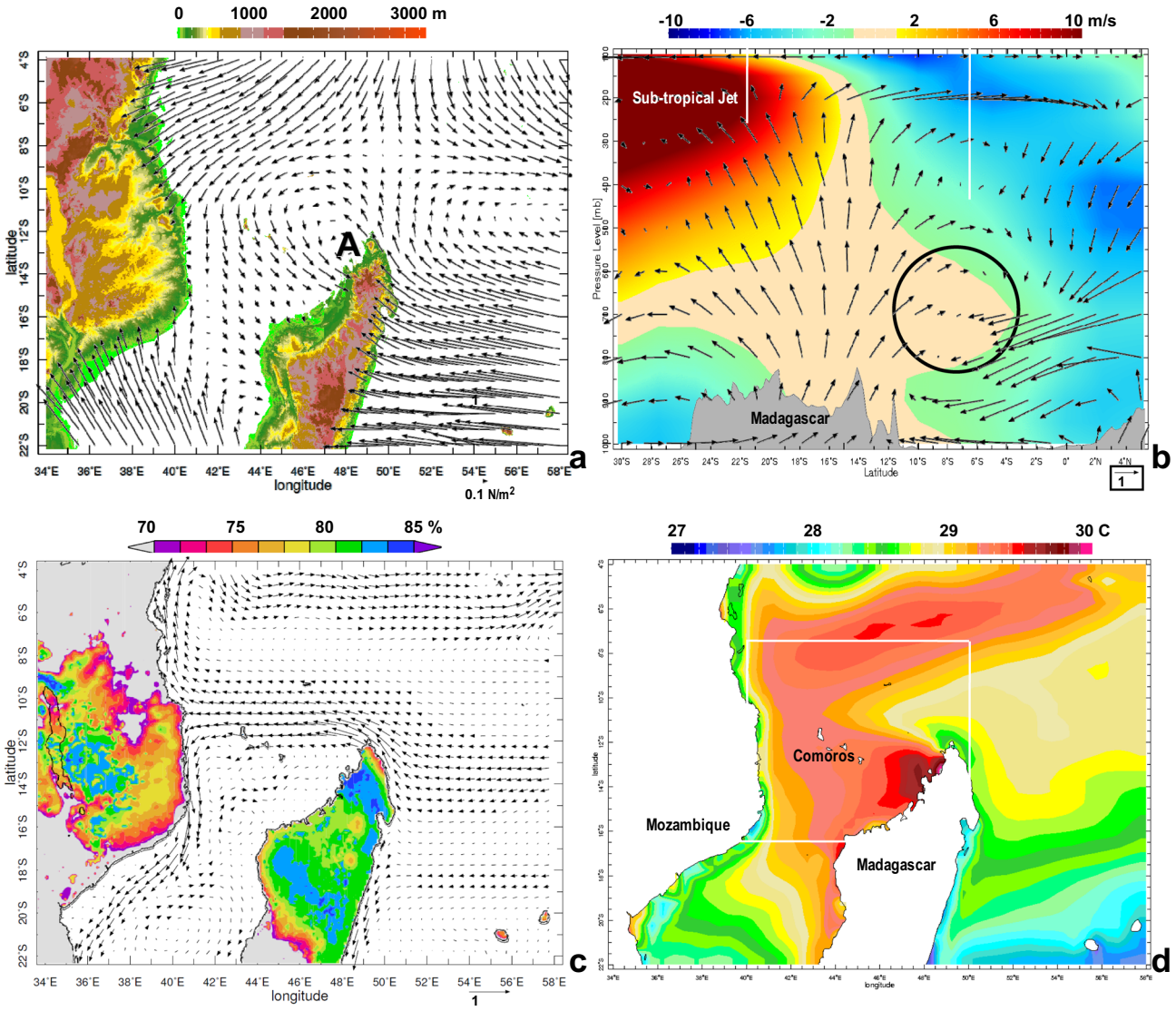


Fig. 1 Dec–Apr climatology of: **a** SODA3 marine wind stress and topography (shaded), A = standing wind rotor. **b** North–south height section along 45°E of NCEP2 meridional circulation (vectors) and zonal wind (shaded); circle highlights absence of westward flow; topographic profile given. Dec-Apr climatology of: **c** SODA3 near-surface ocean currents and FLDAS soil moisture (> 70% shaded), **d** NASA SST and nMC target (box)

standing wind rotors and a leeward trough (Barimalala et al. 2018). The mean circulation analyzed in N–S height section (Fig. 1b) shows low-level convergence and uplift in the inter-tropical trough and an upper-level westerly jet in the sub-tropics. The mean summer circulation reflects an absence of easterly flow in the 800–600 layer hPa over the nMC, consistent with earlier studies (Moore 2013).

The regional oceanography is dominated by the South Equatorial Current which passes the northern tip of Madagascar and (Fig. 1c) then diverges along the east African coast, shedding eddies toward Mozambique (Jury 2018b). Winds and currents are weak in the nMC so heat accumulates there despite export and evaporation (Fig. 1d). Anticyclonic wind stress curl northwest of Madagascar promotes downwelling and SST > 30 °C in a NW axis through the Comoros (Malan et al. 2013).

The circulation needed to steer TCs westward through the nMC often relates to Pacific La Niña according to Vitart et al. (2003). Examining 500 hPa zonal winds, a significant easterly trend is evident (Fig. 2a) interspersed with 2–6 year oscillations. Lead/lag correlations show significant associations with global and regional indices at 2–3 month lag (Fig. 2a,b), being negative for SOI and positive for Niño3.4 and IOD. The correlations infer that Pacific cool phase (La Niña) and cool-west phase Indian dipole associate with westward steering flow (-U). Although mostly in-phase, Pacific

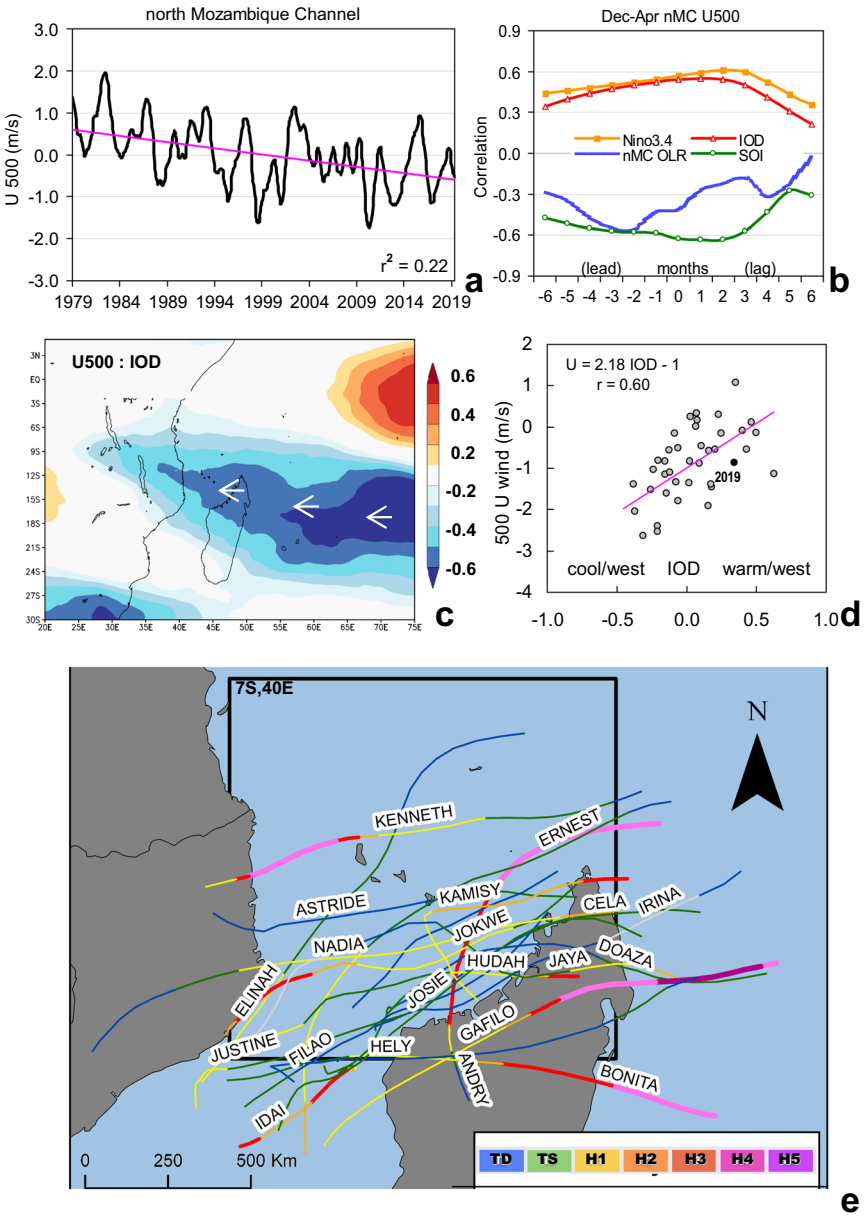


Fig. 2 **a** Filtered nMC 500 hPa zonal (U) wind anomalies and trend. **b** Lag correlation of Dec–Apr seasonal nMC U500 values with global ENSO and regional indices ($N=40$). **c** Regression of seasonal IOD values onto ERA5 Dec–Apr U500 field and **d** scatterplot of Dec-Apr seasonal nMC U500 vs IOD with 2019 labeled. **e** Tracks and intensity of TC in the north Mozambique Channel (nMC) since 1979, shown within the period –1 to + 1 days from date in Table 3. The study region is denoted by the black box

and Indian Ocean Rossby wave oscillations can decouple (Lin 2009).

Table 2 lists the seasonal climate conditions ranked by westward steering flow. There appears to be little coherence in values. Increased convection (-OLR) and easterly flow does not guarantee frequent westward moving TC in the nMC. Reasons for this dichotomy emerge in Fig. 2c, d. Under cool/west dipole conditions (–IOD) the Dec–Apr steering flow tends to be westward (scatterplot $r=0.60$). Yet TC energy sources are limited by oceanic upwelling during –IOD, which is phase-locked to early summer (Appendix Fig. 9a). Seasonal correlations with nMC TCs are weak. Although TC density east of Madagascar associates with IOD and ENSO (Ash and Matyas 2012), Dec–Apr convection (-OLR) in the nMC correlates insignificantly with global indices: $r=-0.22$ IOD, 0.16 SOI, -0.12 Niño3.4. This finding is consistent with Ho et al. (2006), that ENSO affects TC genesis around 70°E but not further west (eg. nMC). Given the weak interannual relationships between TC activity and environmental conditions, the intra-seasonal time scale demands attention.

3.2 Daily composites and MJO influence

The tracks and intensity of westward moving TCs transiting the nMC area 1979–2019 are illustrated in Fig. 2e. There are 21 TCs in the period (cf. Table 3) after screening out weak recurving cases. Daily environmental conditions

Table 2 Ranks for Dec–Apr seasons with mid-level easterly flow (− U) and associated variables: 500 hPa omega (− w), Precipitable water, SST, convection index (OLR) within the nMC study area. Dates according to January, number preceding years are # TC passing through the nMC. TC are absent in many years, regardless of seasonal conditions

Ranked	500 U	Prec.wt	500 -w	SST	OLR
1999	−3.5	47.6	−0.025	29.0	240.8
2–2000	−2.7	45.2	−0.012	28.7	248.1
2001	−2.6	48.2	−0.030	28.9	241.8
2006	−2.1	49.6	−0.028	29.0	239.5
1981	−1.6	47.0	−0.022	28.8	248.5
2009	−1.5	49.0	−0.022	29.3	236.0
2011	−1.4	49.5	−0.026	29.1	236.0
2017	−1.4	50.3	−0.034	29.2	235.1
1–1996	−1.2	48.9	−0.037	29.0	235.2
2–1984	−1.2	49.2	−0.051	28.5	230.2
3–1988	−1.0	48.7	−0.022	29.4	241.5
2010	−1.0	51.0	−0.024	29.6	238.9
1986	−0.9	48.1	−0.033	28.7	236.3
1998	−0.8	53.0	−0.033	29.6	234.3
2–2019	−0.8	51.7	−0.036	29.5	231.9

underpinning these events are composited in Fig. 3a–c. An anomalous 500 hPa subtropical ridge 35°S, 50°E contributes to westward motion and inhibits southward recurvature. Normally, the Mascarene high is located east near 30°S, 75°E (Bessafi and Wheeler 2006). The average latitude (longitude) of formation for the 21 TCs is 11°S (65°E); the composite storm passes north of Madagascar in the sequence from –2 to + 2 days (Fig. 3a). Fifteen of the TCs make landfall over the east coast of Madagascar. Nine make landfall over Mozambique, with four others passing within 50 km of its coast. Composite low level winds (Fig. 3b) reflect a 5 m/s surge of the NW monsoon in the nMC, while composite upper winds (Fig. 3c) illustrate anticyclonic ridging of the subtropical jet and 7 m/s anomalous SE flow near Mauritius (25°S, 60°E) that steers TCs toward the nMC.

The MJO influence on nMC TC formation is studied using methodology from Ho et al. (2006) to reveal cyclogenesis in austral summer under phase-2 (eg. convection moving from Africa to the Indian Ocean). The 21-event composite MJO-filtered OLR anomaly (Fig. 4a) shows negative and then positive excursions that grow in intensity from 20°E to 70°E. Amongst the 21 events, six TCs occurred with strong MJO convective signal at 70°E (eg. OLRa < -2 W/m^2) and another four TCs followed strong MJO convection at 20°E. We infer that MJO have a role in the development of nMC

Table 3 West-moving TC in the nMC: name, central date (yyyy mm dd), marine wind speed squared, maximum rain (mm), central pressure, 500 hPa zonal wind, and track heading within the nMC area

TC	nMC date	spd^{2}W*	Rain*	Press*	U 500	Track°
Benedicte	1981 12 21	323	193	1004.4	1.0	240
Justine	1982 03 21	211	138	1003.6	−2.1	252
Elinah	1983 01 11	177	109	1009.6	−4.3	225
Andry	1983 12 11	106	203	1007.4	−4.7	205
Kamisy	1984 04 10	468	296	994.5	1.1	280
Doaza	1988 01 26	245	427	998.7	1.6	250
Filao	1988 02 26	263	187	1005.1	−1.7	235
Hely	1988 03 28	105	123	1005.9	0.3	260
Nadia	1994 03 24	484	192	1002.7	−4.4	262
Bonita	1996 01 11	168	172	1003.1	5.9	270
Josie	1997 02 10	289	199	1004.9	1.9	242
Astride	2000 01 02	134	131	1008.1	−3.9	268
Hudah	2000 04 04	315	161	1006.3	−4.6	260
Cela	2003 12 10	106	120	1009.5	−2.5	245
Gafilo	2004 03 07	392	235	992.9	4.5	250
Ernest	2005 01 20	242	108	1006.8	−2.5	232
Jaya	2007 04 05	202	148	1009.1	−3.8	265
Jokwe	2008 03 07	375	202	1003.6	−2.7	248
Irina	2012 02 27	266	197	999.4	4.0	253
Idai	2019 03 11	272	111	1003.6	−1.0	205
Kenneth	2019 04 24	391	192	1003.9	−3.6	259

These cases form the composite in Fig. 3. Values listed are from the TC database and (*) refers to EC5 reanalysis peak value over sea

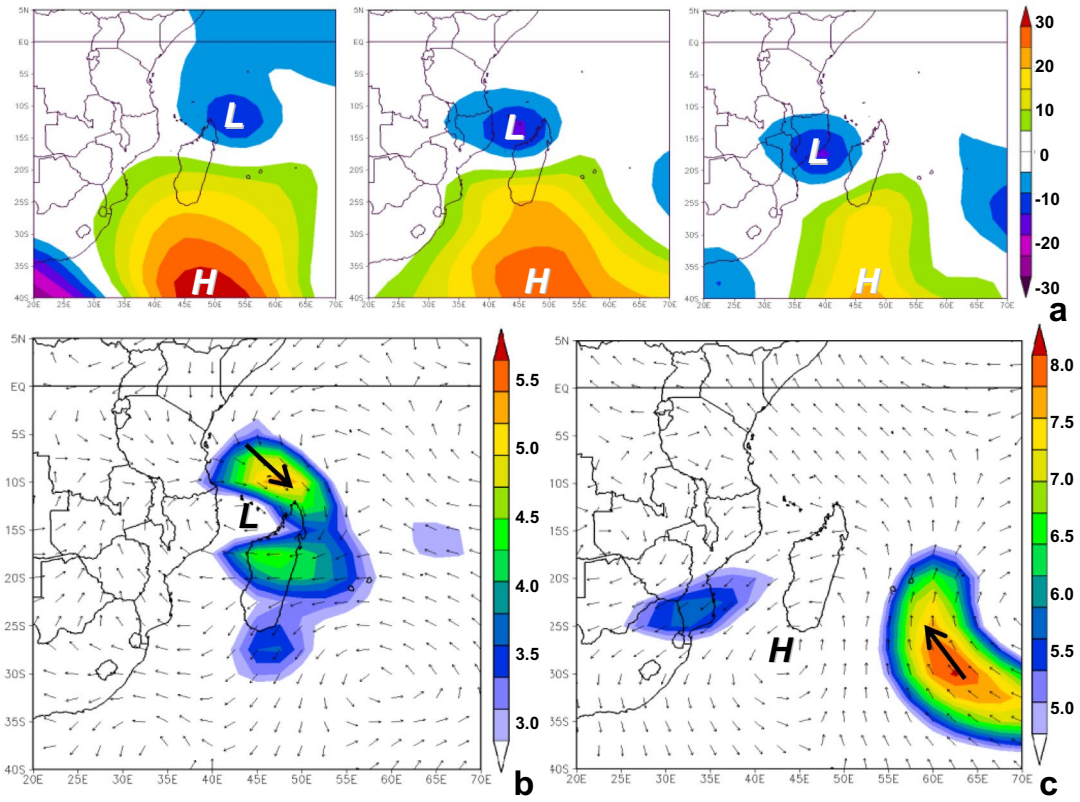


Fig. 3 Composite maps of 21 days with westward nMC TC (cf. Table 3): **a** NCEP2 500 hPa geopotential height anomaly (m) day 2, day 0, day + 2 (left to right), **b**,**c** NCEP2 925 and 200 hPa wind anomaly (m/s) on day 0

TC which depends on how they intensify and interact with the monsoon and IOD.

The filtered OLR lag-correlation function (Fig. 4b) grows in amplitude from October to March, as MJO intensify across the Indian Ocean, thus having more influence near the end of the TC season. Correlating the austral summer African MJO with the sea level air pressure field (Fig. 4c,d) a signal emerges over the Indian Ocean at day–12 (high) and day + 12 (low), consistent with ~ 5.3 m/s average propagation of MJO from 20°E to 70°E. This work is relevant to early 2019 (cf. Appendix Fig. 9b) wherein the RMM amplitude–phase diagram shows high amplitude MJO entering the West Indian Ocean coinciding with nMC TC occurrence.

3.3 Anomalous nature of Jan–Apr 2019

We consider west–east sections of tropical air–sea anomalies in Jan–Apr 2019 in Fig. 5a,b. The Walker Cell and downwelling ocean Rossby wave heralded the onset of warm phase + IOD. Sinking (70°E) / rising (45°E) airflow was connected by deep easterlies over subsurface temperature anomalies > 2 °C. The NDBC buoy northeast of Madagascar (8°S, 5°5E) recorded SST rising from 28 °C to 31 °C in Jan–Apr 2019. Westward steering flow across a dry (70°E) —moist (45°E) dipole promoted TCs in the nMC. Hovmoller analysis of sea surface height (SSH) along 10°S (Fig. 5c) indicates that an ocean Rossby wave propagated westward at ~ 0.2 m/s from Sumatra (Jun 2018) to Madagascar (Feb 2019). The anomalous high SSH brought warmer SST and atmospheric convection to the west Indian Ocean, followed by a second wave in late 2019, fully establishing + IOD conditions.

Marine conditions 10–20 Apr 2019 (Fig. 6a) reveal > 31 °C sea temperatures northwest of Madagascar where prior wet spells resulted in salinity < 34.5 ppt. Westward ocean currents along 10°S generated anticyclonic shear and downwelling in the nMC area. SST > 31 °C in the west Indian Ocean are rare, given heat export by the South Equatorial Current and cooling by monsoon winds (Schott et al. 2009). Hovmoller plots averaged 7–17°S of rainfall and mid-level humidity (Fig. 6b,c) reveal 4.4 m/s westward movement of moist convection from 70°E to 40°E over the period 17–27 Apr 2019. This feature is structurally consistent with the moist envelope of a slow easterly wave (Burpee 1972) which surrounds TCs and enables cloud heating.

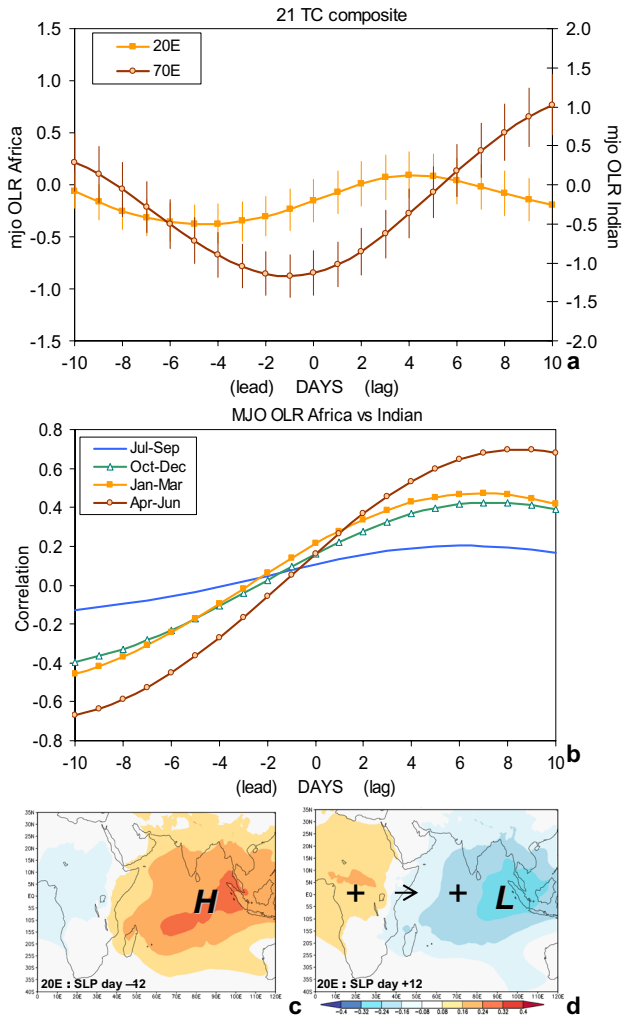


Fig. 4 **a** 21 case composite MJO amplitude 10 days before to after nMC TC (day-0 listed in Table 3). **b** Lag correlation of MJO netOLR 70°E vs 20°E by season $N = 6000$. **c**,**d** Regression of Dec–Apr 20°E MJO netOLR with ERA5 sea level air pressure field at lag –12 (left) and + 12 days (right); with MJO index center-points denoted by plus symbols

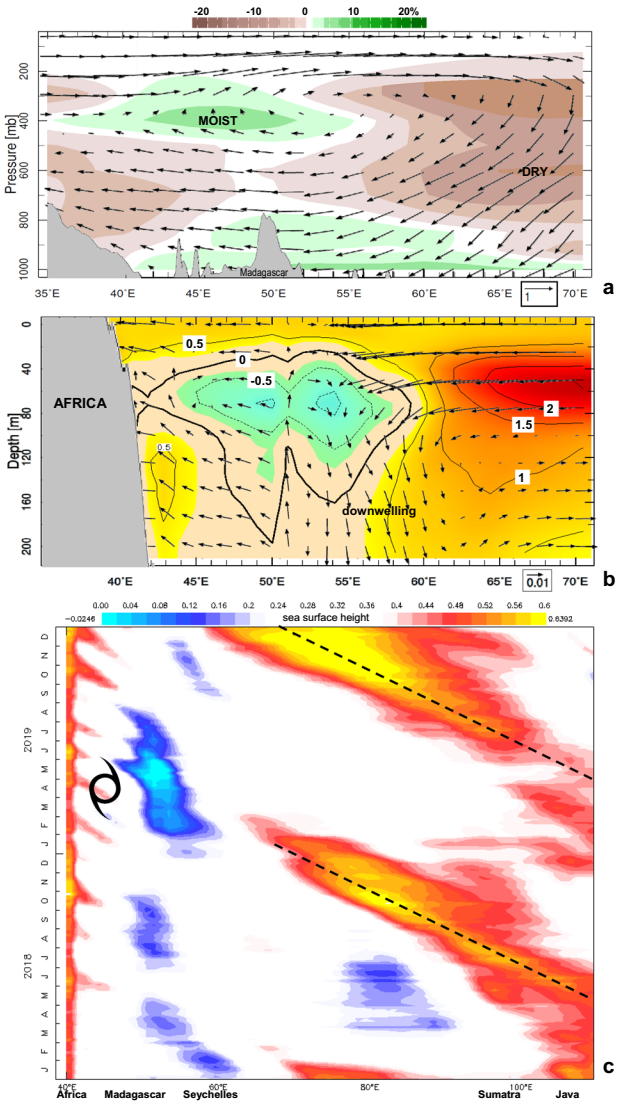


Fig. 5 West–east section on 7–17°S of Jan–Apr 2019 anomalies: **a** NCEP2 atmospheric circulation and humidity with topographic profile, and **b** GODAS ocean circulation and temperature, vertical motion exaggerated. **c** Hovmoller analysis on 10°S of GODAS sea surface height illustrating westward ocean Rosby waves in 2018–19. Dashed lines indicate a phase speed ~ 0.2 m/s, TC icon denotes Kenneth

3.4 TC event conditions

The local TC warning center (Meteo-France Reunion) noticed a disturbance had formed on 21 Apr 2019 and began issuing warnings on Kenneth by 23 Apr. It intensified rapidly prior to landfall near Pemba, Mozambique at 1315 UTC on 25 Apr, maintaining a westward trajectory across the nMC.

The atmospheric circulation during intensification of TC Kenneth included low-level westerlies north of the vortex, trade winds to south and a retro-grading subtropical high pressure cell (Fig. 7a). Upper easterlies strengthened north of Madagascar, and sub-tropical westerlies altered from trough on 21 Apr to ridge on 24 Apr; a feature of MJO influence (Ho et al. 2006) which diverted the sub-tropical jet. The 150-hPa ozone map at 12 UTC 24 Apr 2019 (Fig. 7b) indicates two spiral bands ($O3 < 50$ ppb) and divergent upper outflow west of the system. Such low ozone values reflect deep upward motions associated with TC passage (Zou and Wu 2005; Jenkins et al. 2015, Minschwaner et al. 2015). Ocean swells reached 7 m as TC Kenneth passed the Comoros at 12.4°S, 43.4°E with wave direction from 60 to

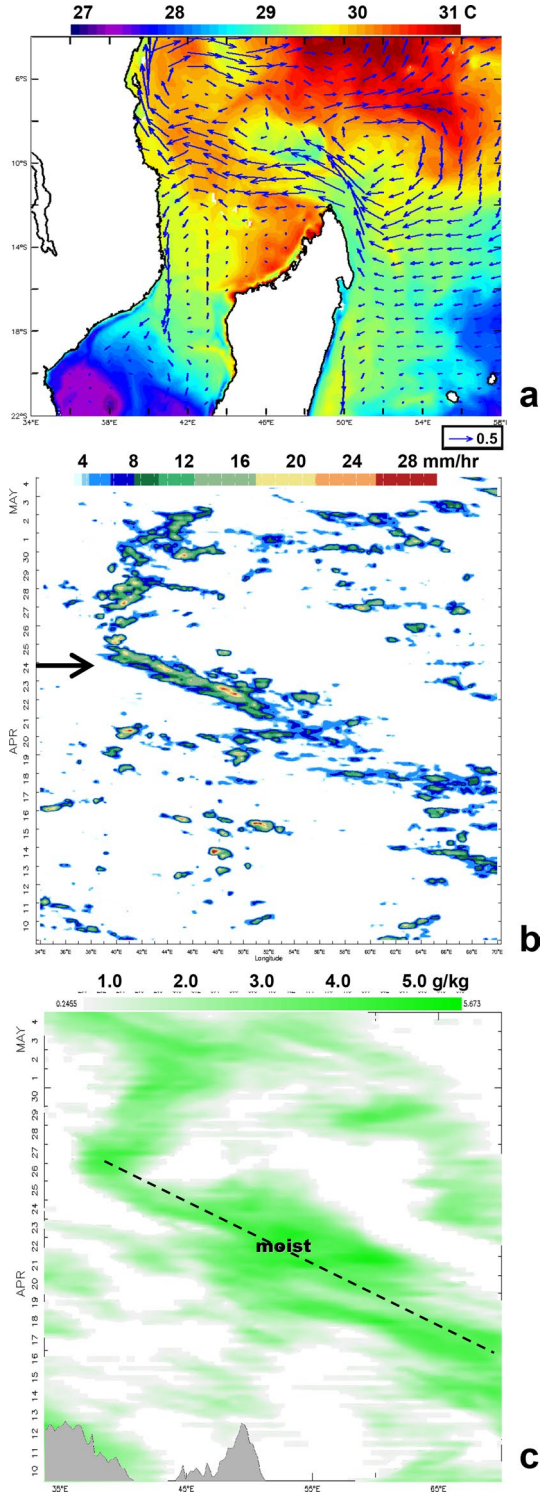


Fig. 6 10–20 April 2019 averaged maps of: **a** HYCOM SST and surface currents. Hovmoller plots 10 Apr – 5 May 2019, averaged over 7–17°S of: **b** cMorph maximum 3-hourly rainfall; MERRA2 6-hourly: **c** 500 hPa specific humidity. Arrow in b) points to 24 Apr 2019, time goes up, topographic profile illustrated in **c** lower; dashed line highlights 4.4 m/s propagation of the moist envelope consistent with an 'easterly wave'

80° and period of 10 s (Fig. 7c,d). A pressure minimum of 957 hPa contributed to 3 + m storm surge, damaging east-facing coasts. An analysis of the air–sea interactions underpinning TC Kenneth is given in Mawren et al. (2020)

Reanalysis maximum winds reached 22 m/s consistent with FMCZ-observed gusts (Fig. 8a, MeteoFrance Reunion 2019). ERA5 exhibited a single peak of wind 12–20 UTC 24 Apr while CFS2 showed 3–4 oscillations from 16 UTC 24th to 08 UTC 25th. Rain rates peaked at 30 mm/hr at 49°E on 23 Apr and again at 43°E on 24 Apr during transit of the nMC. After landfall the TC remnants caused heavy rains on 40°E from 27 to 30 Apr 2019. The weather station at Pemba in Cabo Delgado recorded 424 mm (WMO 2019). Reanalysis rain of 6–8 mm/hr (Fig. 8b) compared favourably with GPM peaks of 8–10 mm/hr a few hours earlier.

Numerical models predicted TC Kenneth formation, westward track and intensification (Fig. 8c,d). One model recurved to Madagascar, but eight models forecast Mozambique landfall within 100 km of 12°S at 2-day lead. Five models correctly forecast the storm to linger over the coastal plains causing floods. Two models under-forecast maximum winds while three models correctly predicted ~ 60 m/s at 0 UTC 25 Apr 2019. Ensemble forecasts from HWRF over the period 21–27 Apr (Fig. 8d lower) revealed 3 members southward, 6 northward and 11 becalmed near Pemba. The range of HWRF forecasts for landfall was + /–6 h and for Pmin was + /–10 hPa. Good model performance may be attributed to the shielding effect by the southern spiral band from the sub-tropical jet (cf. Fig. 7b). Vertical sections of COTC model 6-h forecasts (Fig. 8e,f) indicate that Kenneth had stronger winds and higher humidity on its left (poleward) flank. Anomalous heating > 5 °C was predicted in the 550–250 hPa layer during intensification on 12 UTC 24 Apr 2019. Although advance warnings were issued, many people in the Comoros and northern Mozambique suffered TC impacts, as noted in Mawren et al. (2020).

4 Summarizing discussion

The tropical cyclone season of Dec 2018 to Apr 2019 in the southwest Indian Ocean was the costliest ($2.3B), deadliest (1382) and most active season in the historical era, with 9 TC exceeding category 2 and 6 TC tracking westward over 1000 km (Masters 2019). This prompted a study of westward-moving TC in the northern Mozambique Channel. We examined conditions from longer to shorter time scales, ultimately focusing on TC Kenneth in April 2019. Analysis at longer time scale determined that Pacific La Niña and –IOD promote westward steering flow but tend to limit thermodynamic energy and convection. However, MJO entering the west Indian Ocean trigger TC formation

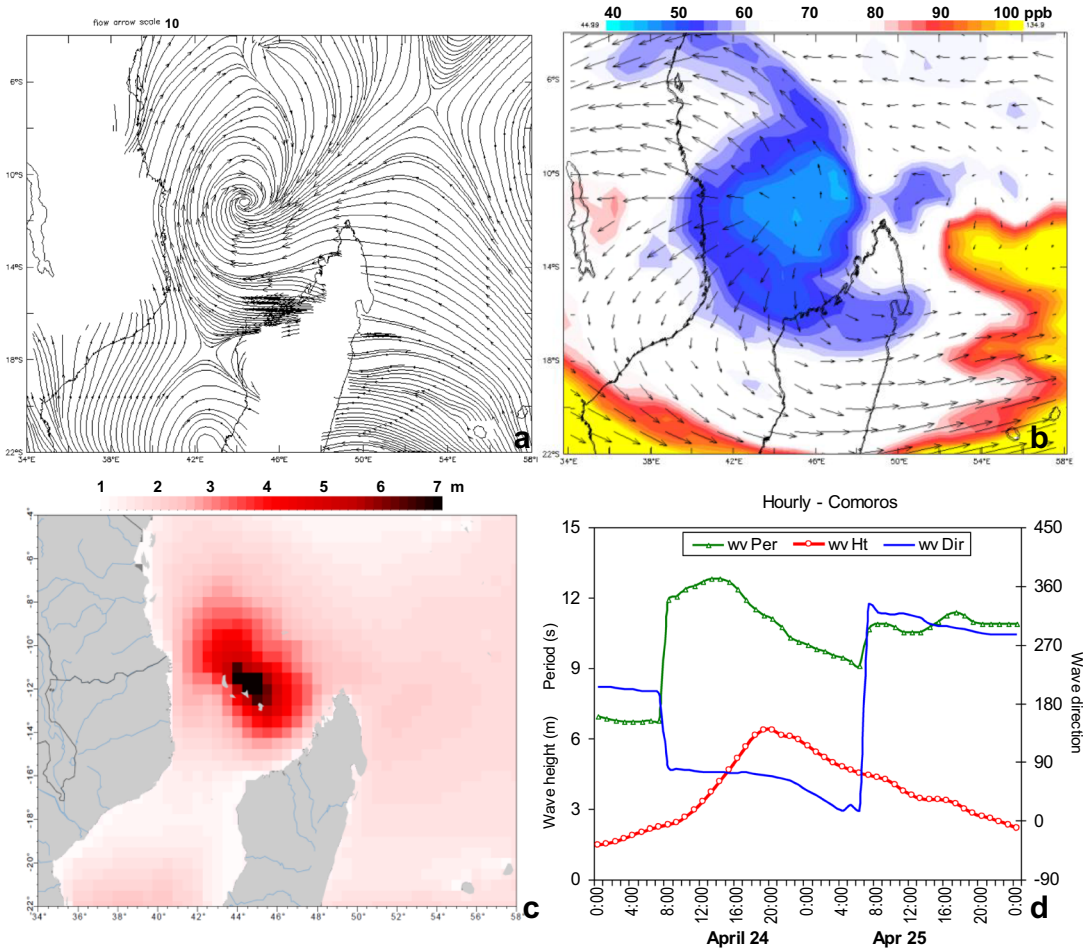


Fig. 7 MERRA2 maps of 12 UTC 24 Apr 2019: **a** 975 hPa streamlines, **b** 150 hPa wind vectors and ozone (shaded). **c** Wavewatch3 significant wave height map at 12 UTC 24 Apr 2019 and **d** hourly wave conditions at virtual station in Comoros (12.4S, 43.4E)

and subtropical ridging that promotes movement toward the nMC, particularly at the end of austral summer.

Conditions in early 2019 favoured westward steering flow over Madagascar. The onset of + IOD was evident in the Walker circulation, downwelling ocean Rossby wave and SST > 31 °C northwest of Madagascar. Two strong MJO entered the west Indian Ocean triggering the formation of TC Idai (March) and Kenneth (April) which transited the Mozambique Channel causing unprecedented floods.

The case study of TC Kenneth in the Comoros Islands used reanalysis products to document waves of 7 m contributing to storm surge > 3 m. Reanalysis winds of 22 m/s were about half the maximum estimated by vortex-scale models and the local TC warning center. Satellite rainfall and upper level ozone revealed a southern spiral cloud band (cf. Fig. 7d) shielding the TC from subsidence and anticyclonic vorticity of the sub-tropical jet over Madagascar. Numerical models predicted the westward track and intensification of TC Kenneth 23–25 Apr 2019; less than one-third of forecast tracks recurved away from landfall at 12°S, 40°E. Further work will consider whether the anomalous weather of 2019 may be harbinger of future climate in the Southwest Indian Ocean.

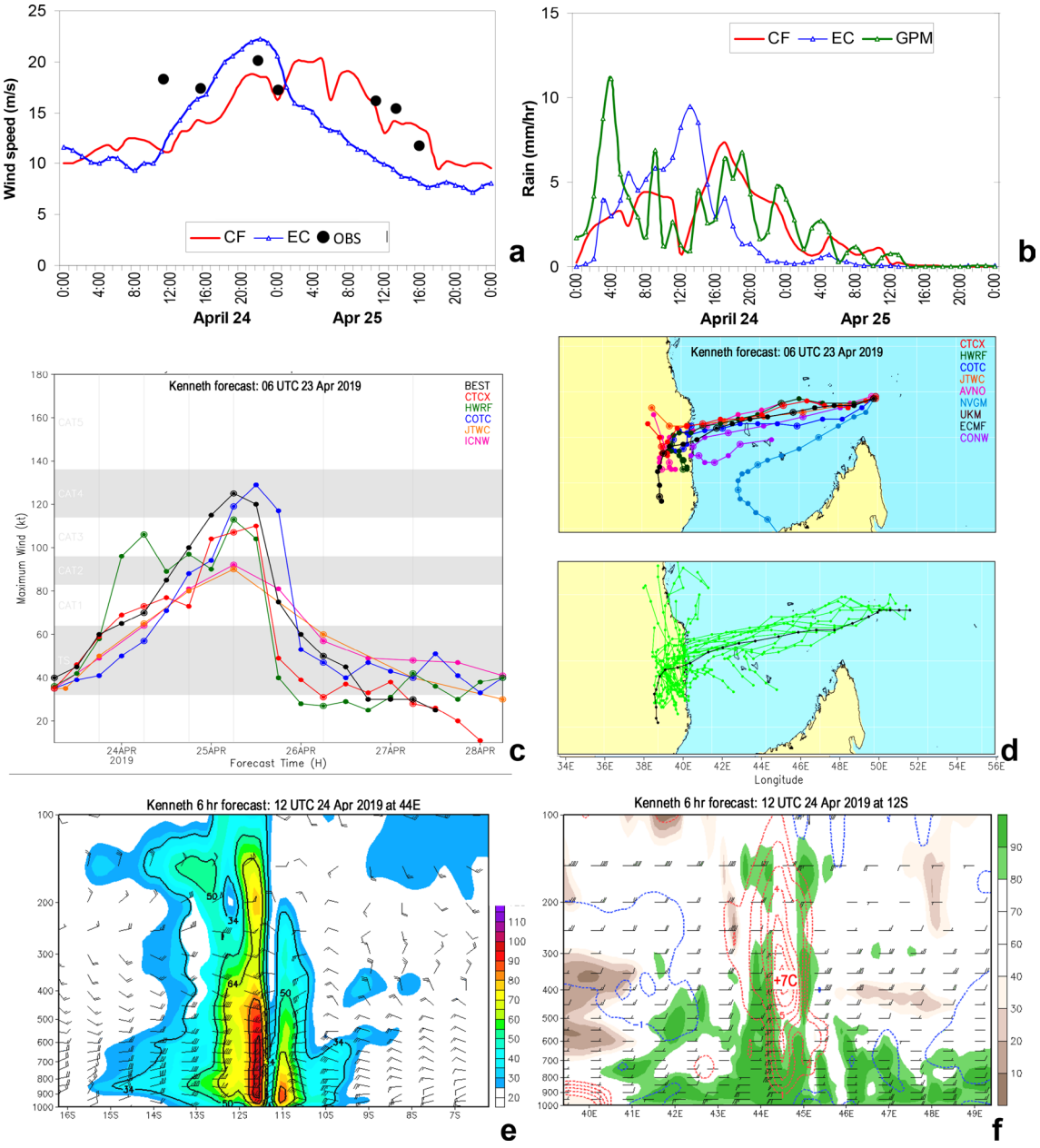
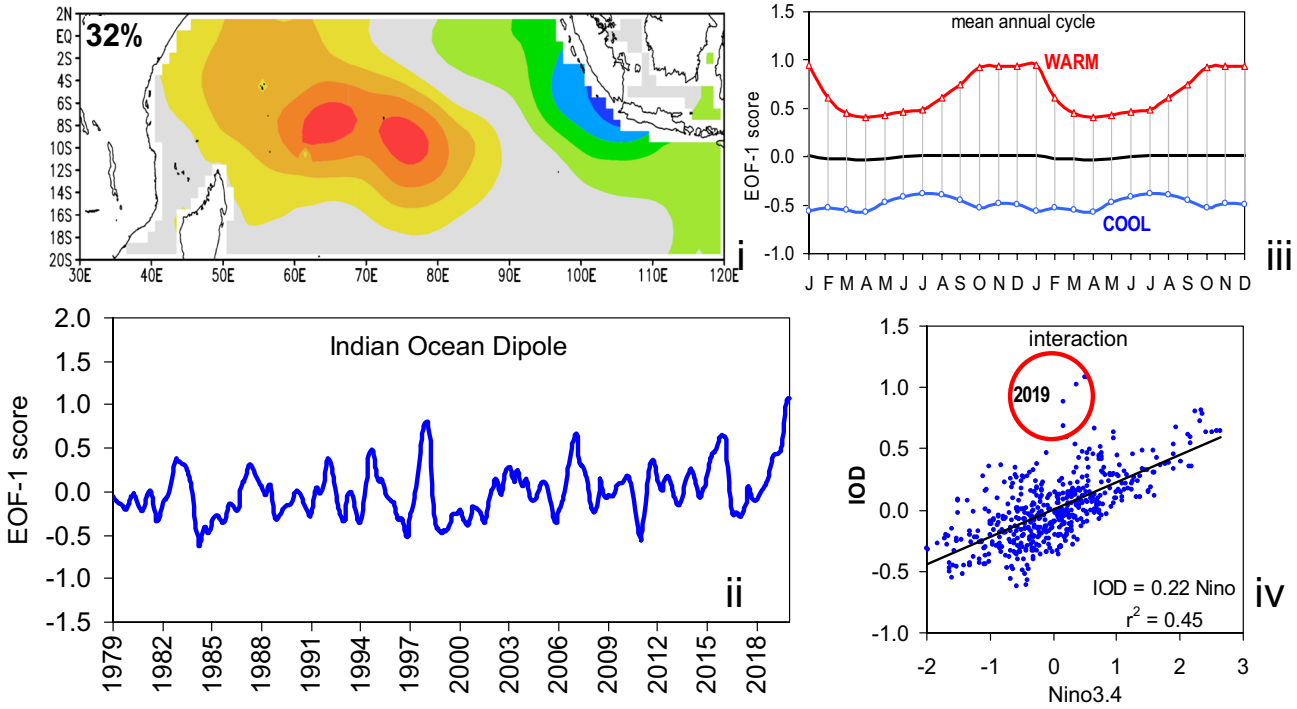


Fig. 8 Hourly time series at Comoros virtual station (12.4°S, 43.4°E) comparing ERA5 and CFS2 wind speed and rainfall (right), with FMCZ-observed gusts and GPM satellite. Tropical cyclone Kenneth multi-model forecasts: **c** wind intensity and **d** tracks (HWRF ensemble green, lower) compared with observed 'best' (black w/dots). COTC vortex-scale 6 h forecast valid 12 UTC 24 Apr 2019 of e) north–south height section of wind (m/s) and f) east–west height section of wind, humidity (%) and heating (°C)

Appendix

See below Fig. 9.

a Representing the IOD with 1-100 m sub-surface sea temperatures south of the equator: i) Empirical orthogonal function mode-1 loading pattern and ii) filtered time score, iii) mean annual cycle segregated into warm and cool phase, and iv) IOD vs Nino3.4 scatterplot and regression. Red circle indicates 2019 IOD was decoupled from the Pacific.



b Global MJO RMM diagram Apr-Jun 2019 (Wheeler and Hendon 2004); black dot (below left) denotes the genesis of TC Kenneth in the nMC.

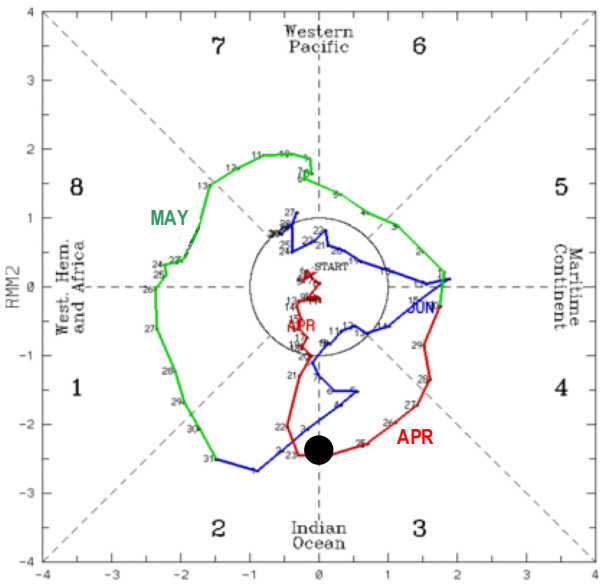


Fig. 9 **a** Representing the IOD with 1–100 m sub-surface sea temperatures south of the equator: (i) Empirical orthogonal function mode-1 loading pattern and (ii) filtered time score, (iii) mean annual cycle segregated into warm and cool phase, and (iv) IOD vs Nino3.4 scatterplot and regression. Red circle indicates 2019 IOD was decoupled from the Pacific. **b** Global MJO RMM diagram Apr–Jun 2019 (Wheeler and Hendon 2004); black dot (below left) denotes the genesis of TC Kenneth in the nMC

Acknowledgements Satellite, reanalysis and vortex-scale model data were obtained from Univ Hawaii APDRC, KNMI Climate Explorer, IRI Climate Library, NOAA Coastwatch, Navy Coamps-TC. The first author acknowledges on-going support from the SA Dept of Education.

Data Availability A data spreadsheet is available on request, including much of the analysis here, url links to websites for data and macro subroutines employed in statistical processing and analysis.

References

Ash KD, Matyas CJ (2012) The influences of ENSO and the Subtropical Indian Ocean dipole on tropical cyclone trajectories in the South Indian Ocean. Intl J Climatol 32:41–56

Barimalala R, Desbiolles F, Blamey RC, Reason C (2018) Madagascar influence on the South Indian Ocean convergence zone, the Mozambique channel trough and Southern African rainfall. Geophys Res Letters 45:11380–11389

Behringer DW (2007) The global ocean data assimilation system (GODAS) at NCEP. Proc 11th Symp on Integrated Observing and Assimilation Systems, San Antonio TX, Amer Meteor Soc:3.3

Bessafi M, Wheeler MC (2006) Modulation of south Indian Ocean tropical cyclones by the Madden-Julian Oscillation and convectively coupled equatorial waves. Mon Weather Rev 134:638–656

Burns JM, Subrahmanyam B, Nyadjro ES, Murty VSN (2016) Tropical cyclone activity over the southwest tropical Indian Ocean. J Geophys Res Oceans 121:6389–6402

Burpee RW (1972) The origin and structure of easterly waves in the lower troposphere in North Africa. J Atmos Sci 29:77–90

Carton JA, Chepurin GA, Chen L (2018) SODA3: A new ocean climate reanalysis. J Climate 31:6967–6983

Cattiaux J, Chauvin F, Bousquet O, Malardel S, Tsai C (2020) Projected changes in the southern Indian Ocean cyclone activity assessed from high-resolution experiments and CMIP5 Models. J Climate 33:4975–4991

Chang-Seng D, Jury MR (2010a) Tropical cyclones in the SW Indian Ocean. Part 1: inter-annual variability and statistical prediction. Meteorol Atmos Phys 106:149–162

Chang-Seng D, Jury MR (2010b) Tropical cyclones in the SW Indian Ocean. Part 2: structure and impacts at the event scale. Meteorol Atmos Phys 106:163–178

Chikoore H, Vermeulen JH, Jury MR (2015) Tropical cyclones in the Mozambique channel: January–March 2012. Nat Hazards. https://doi.org/10.1007/s11069-015-1691-0

Cretat J, Terray P, Masson S, Sooraj KP (2018) Intrinsic precursors and timescale of the tropical Indian Ocean Dipole: insights from partially decoupled numerical experiment. Climate Dyn 51:1311–1332

Doyle JD, Hodur RM, Chen S, Jin Y, Moskaitis JR, Wang S, Hendricks EA, Jin H, Smith TA (2014) Tropical cyclone prediction using COAMPS-TC. Oceanography 27:104–115

Dyson LL, vanHeerden J (2001) The heavy rainfall and floods over the northeastern interior of South Africa during February 2000. S Afr J Science 97:80–86

Emanuel KA, Nolan DS (2004) Tropical cyclone activity and global climate. 26th Conf Hurr Tropical Meteorol, Miami FL, Amer Meteor Soc:240–241

Fitchett JM, Grab SW (2014) A 66-year tropical cyclone record for south-east Africa, temporal trends in a global context. Intl J Climatol:doi. https://doi.org/10.1002/joc.3932

Hersbach H (2020) The ERA5 global reanalysis. Quart J Roy Meteor Soc 146:1999–2049

Ho CH, Kim JH, Jeong JH, Kim HS, Chen DL (2006) Variation of tropical cyclone activity in the South Indian Ocean: El Nino-Southern oscillation and Madden-Julian oscillation effects. J Geophys Res Atmos. https://doi.org/10.1029/2006jd007289

Hou AY, Kakar RK, Neeck S, Azarbarzin AA, Kummerow CD, Kojima M, Oki R, Nakamura K, Iguchi T (2014) The global precipitation measurement mission. Bull Amer Meteor Soc 95:701–722

Huffman GJ, Adler RF, Bolvin DT, Gu G, Nelkin EJ, Bowman KP, Hong Y, Stocker EF, Wolff DB (2007) The TRMM multi-satellite precipitation analysis (TMPA): quasi-global, multiyear, combined-sensor precipitation estimates at fine scales. J Hydrometeor 8:38–55

Hurlburt HE (2009) High resolution global and basin-scale ocean analyses and forecasts. Oceanography 22:110–127

Izumo T, Vialard J, Lengaigne M, deBoyer-Montégut C, Behera SK, Luo JJ, Cravatte S, Masson S, Yamagata T (2010) Influence of the state of the Indian Ocean dipole on following year's El Niño. Nature Geosci 3:168–172

Jenkins GS, Robjhon ML, Reyes A, Valentine A, Nieves L (2015) Elevated middle and upper troposphere ozone observed downstream of Atlantic tropical cyclones. Atmos Environ 118:70–86

Joyce RJ, Janowiak JE, Arkin PA, Xie PP (2004) CMORPH: a method that produces global precipitation estimates from passive microwave and infrared data at high spatial and temporal resolution. J Hydrometeor 5:487–503

Jury MR (1993) A preliminary study of climatological associations and characteristics of tropical cyclones in the SW Indian Ocean. Meteorol Atmos Phys 51:101–115

Jury MR (2013) Variability in the tropical southwest Indian Ocean and influence on Southern Africa climate. Intl J Marine Sci 3:46–64

Jury MR (2016) Summer climate of Madagascar and monsoon pulsing of its vortex. Meteorol Atmos Physics 128:117–129

Jury MR (2018a) South Indian Ocean Rossby waves. Atmos Ocean 56:322–331

Jury MR (2018b) Modulation of currents near Durban. Reg Stud Marine Sci 18:208–218

Jury MR, Huang B (2004) The Rossby wave as a key mechanism of Indian Ocean climate variability. Deep Sea Res 51:2123–2136

Jury MR, Pathack B, Parker B (1998) Climatic determinants and statistical prediction of tropical cyclone days in the southwest Indian Ocean. J Climate 12:1738–1746

Kanamitsu M, Ebisuzaki W, Woollen J, Yang SK, Hnilo JJ, Fiorino M, Potter GL (2002) NCEP-DOE AMIP-2 Reanalysis. Bull Amer Meteor Soc 83:1631–1643

Kiladis GN, Dias J, Straub KH, Wheeler MC, Tulich SN, Kikuchi K, Weickmann KM, Ventrice MJ (2014) A comparison of OLR and circulation-based indices for tracking the MJO. Mon Wea Rev 142:1697–1715

Leroux M, Meister J, Mekies D, Dorla A, Caroff P (2018) A climatology of southwest Indian Ocean tropical systems: their number, tracks, impacts, sizes, empirical maximum potential intensity, and intensity changes. J Appl Meteor Climatol 57:1021–1041

Lin J (2009) Ocean-atmosphere interaction in the lifecycle of ENSO: The coupled wave oscillator. Chin Ann Math Ser B 30:715–726

Lin Z (2019) The south Atlantic-south Indian Ocean pattern: a zonally oriented teleconnection along the southern hemisphere westerly jet in austral summer. Atmosphere. https://doi.org/10.3390/atmos10050259

Luo J-J, Zhang R, Behera SK, Masumoto Y, Jin F-F, Lukas R, Yamagata T (2010) Interaction between El Niño and extreme Indian Ocean dipole. J Climate 23:726–742

Madden RA, Julian PR (1994) Observations of the 40–50 day tropical oscillation – A review. Mon Wea Rev 122:814–837

Malan N, Reason CJC, Loveday B (2013) Variability in tropical cyclone heat potential over the southwest Indian Ocean. J Geophys Res Oceans 118:6734–6746

Malherbe J, Engelbrecht FA, Landman WA, Engelbrecht CJ (2011) Tropical systems from the southwest Indian Ocean making landfall over the Limpopo River Basin, southern Africa: a historical perspective. Intl J Climatol:doi. https://doi.org/10.1002/joc.2320

Malherbe J, Engelbrecht FA, Landman WA (2012) Projected changes in tropical cyclone climatology and landfall in the southwest Indian Ocean under enhanced anthropogenic forcing. Clim Dyn: https://doi.org/10.1007/s00382-012-1635-2

Malherbe J, Landman WA, Engelbrecht FA (2013) The decadal-scale rainfall cycle, Southern Annular Mode and tropical cyclones over the Limpopo River Basin, southern Africa. Clim Dyn 42:3121–3138

Masters J (2019) Africa's hurricane Katrina: tropical cyclone Idai causes an extreme catastrophe. Weather Underground. <www.wunderground.com/cat6/Africas-Hurricane-Katrina-Tropical-Cyclone-Idai-Causes-Extreme-Catastrophe>

Matyas CJ (2015) Tropical cyclone formation and motion in the Mozambique channel. Intl J Climatol 35:375–390

Matyas CJ, Silva JA (2011) Extreme weather and economic well-being in rural Mozambique. Nature Hazards: https://doi.org/10.1007/s11069-011-0064-6

Mavume AF, Rydberg L, Rouault M, Lutjeharms JRE (2009) Climatology and landfall of tropical cyclones in the south-west Indian Ocean. W Indian Ocean J Marine Sci 8:15–36

Mawren D, Hermes J, Reason CJC (2020) Exceptional tropical cyclone Kenneth in the far northern Mozambique Channel and ocean eddy influences. Geophys Res Lett 47:e2020GL088715

McIntosh PC, Hendon HH (2018) Understanding Rossby wave trains forced by the Indian Ocean dipole. Clim Dyn 50:2783–2798

McNally A, Arsenault K, Kumar S, Shukla S, Peterson P, Wang S, Funk C, Peters-Lidard CD, Verdin JP (2017) A land data assimilation system for sub-Saharan Africa food and water security applications (FLDAS). Scientific Data 4:170012

McPhaden MJ (2009) RAMA: The rsearch Moored Array for African–Asian–Australian Monsoon analysis and prediction. Bull Amer Meteor Soc 90:459–480

Minschwaner K (2015) Signature of a tropical Pacific cyclone in the composition of the upper troposphere over Socorro NM. Geophys Res Lett 42:9530–9537

Molod A, Takacs L, Suarez M, Bacmeister J (2015) Development of the GEOS-5 atmospheric general circulation model: evolution from MERRA to MERRA2. Geosci Model Dev 8:1339–1356

Moore GWK (2013) Impact of the high topography of Madagascar on the structure of the Findlater Jet. Geophys Res Lett 40:2367–2372

Mudenda OS, Mumba ZLS (2004) The unusual storm of January 1996. Proc EUMETSAT meteorological satellite conf, Prague Czech Rep

Poolman E, Terblanche D (1984) Tropical cyclones Domoina and Imboa. SA Weather Bureau Newslett 420:37–45

Reason CJC (2007) Tropical cyclone Dera, the unusual 2000/01 tropical cyclone season in the southwest Indian Ocean and associated rainfall anomalies over southern Africa. Meteor Atmos Phys 97:181–188

Reason CJC, Kiebel A (2004) Tropical cyclone Eline and its unusual penetration and impacts over the southern African mainland. Weather Forecast 19:789–805

ReliefWeb (2019) Document on Cyclone Kenneth <reliefweb.int/report/comoros/comoros-humanitarian-situation-report-no-6-cyclone-kenneth-3-june-2019>

MeteoFrance Reunion (2019) Diagnostic observations of TC Kenneth <www.meteofrance.re/cyclone/saisons-passees/2018-2019/dirre/KENNETH>

Rienecker MM (2011) MERRA: NASA's Modern-Era Retrospective Analysis for Research and Applications. J Climate 24:3624–3648

Saha S (2010) The NCEP Climate Forecast System Reanalysis. Bull Amer Meteor Soc 91:1015–1057

Saji NH, Goswami BN, Vinayachandran PN, Yamagata T (1999) A dipole mode in the tropical Indian Ocean. Nature 401:360–363

Schott FA, Xie S-P, McCreary JP (2009) Indian Ocean circulation and climate variability. Rev Geophys. https://doi.org/10.1029/2007RG000245

Tolman HL, Balasubramaniyan B, Burroughs LD, Chalikov DV, Chao YY, Chen HS, Gerald VM (2002) Development and implementation of wind generated ocean surface wave models at NCEP. Weather Forecast 17:311–333

Vermeulen JH (1995) Tropical cyclones in the southwest Indian Ocean: track prediction and verification 1991–1992. Meteorol Appl 2:217–220

Vitart F, Anderson D, Stockdale T (2003) Seasonal forecasting of tropical cyclone landfall over Mozambique. J Climate 16:3932–3945

Wang B, Elsberry RL, Wang Y, Wu L (1998) Dynamics in tropical cyclone motion: a review. Chin J Atmos Sci 22:416–434

Webster PJ, Moore AM, Loschingg JP, Leben RR (1999) Coupled ocean-atmosphere dynamics in the Indian Ocean during 1997–98. Nature 401:356–360

Wheeler MC, Hendon HH (2004) An all-season real-time multivariate MJO index: development of an index for monitoring and prediction. Mon Wea Rev 132:1917–1932

WMO (2019) document on TC Kenneth <public.wmo.int/en/media/news/another-unprecedented-tropical-cyclone-and-flooding-hits-mozambique>

Xie SP, Annamalai H, Schott FA, McCreary JP (2001) Structure and mechanism of south Indian Ocean climate variability. J Climate 15:864–878

Yeshanew A, Jury MR (2007) North African climate variability, part 1: tropical thermocline coupling. Theor Appl Climatol,. https://doi.org/10.1007/s00704-006-0242-8

Zou X, Wu Y (2005) On the relationship between Total Ozone Mapping Spectrometer ozone and hurricanes. J Geophys Res. https://doi.org/10.1029/2004JD005019

Publisher's Note Springer Nature remains neutral with regard to jurisdictional claims in published maps and institutional affiliations.